DOI: 10.1002/smll.200600689

Large-Scale, Hot-Filament-Assisted Synthesis of Tungsten Oxide and Related Transition Metal Oxide Nanowires

*Jyothish Thangala, Sreeram Vaddiraju, Rahel Bogale, Ryan Thurman, Trevor Powers, Biswapriya Deb, and Mahendra K. Sunkara**

A scalable and versatile method for the large-scale synthesis of tungsten trioxide nanowires and their arrays on a variety of substrates, including amorphous quartz and fluorinated tin oxide, is reported. The synthesis involves the chemical-vapor transport of metal oxide vapor-phase species using air or oxygen flow over hot filaments onto substrates kept at a distance. The results show that the density of the nanowires can be varied from 10^6–10^{10} cm^{-2} by varying the substrate temperature. The diameter of the nanowires ranges from 100–20 nm. The results also show that variations in oxygen flow and substrate temperature affect the nanowire morphology from straight to bundled to branched nanowires. A thermodynamic model is proposed to show that the condensation of WO_2 species primarily accounts for the nucleation and subsequent growth of the nanowires, which supports the hypothesis that the nucleation of nanowires occurs through condensation of suboxide WO_2 vapor-phase species. This is in contrast to the expected WO_3 vapor-phase species condensation into WO_3 solid phase for nanoparticle formation. The as-synthesized nanowires are shown to form stable dispersions compared to nanoparticles in various organic and inorganic solvents.

Keywords:
- arrays
- chemical vapor transport
- metal oxides
- nanowires
- nucleation

1. Introduction

Tungsten trioxide nanomaterials are of great interest due to their potential use as electrochromic, gas sensing, and photocatalyst materials.[1–3] Tungsten oxide nanowires have been synthesized by heating tungsten in various forms (plates, wires, and powders).[4–14] Previously, we reported the synthesis of tungsten oxide and metallic tungsten nanowires using oxygen flow over hot filaments onto substrates maintained at different temperatures.[15] Our study showed that tungsten metal nanowires were formed when condensation of metal oxide vapor-phase species occurred on the substrates that were maintained at temperatures higher than the decomposition of the respective oxide species. Similarly, metal oxide nanowires formed on the substrates that were maintained at temperatures below the decomposition temperature of the respective oxides.[15]

All of the above techniques for the formation of tungsten oxide nanowires involve only vapor–solid interactions, which do not suggest any straightforward reasons for the observed one-dimensional (1D) crystal growth. Specifically,

[*] J. Thangala, S. Vaddiraju, R. Bogale, R. Thurman, T. Powers, B. Deb, Prof. M. K. Sunkara
Department of Chemical Engineering, University of Louisville
Louisville, KY 40292 (USA)
Fax: (+1) 502-852-6355
E-mail: mahendra@louisville.edu

Supporting information for this article is available on the WWW under http://www.small-journal.com or from the author.

the underlying nucleation and growth mechanisms are not understood in terms of how a slight variation within the chemical-vapor-deposition (CVD) setup could yield 1D crystal growth. In the case of low-melting-point metal oxides, the metal itself could provide the medium for either spontaneous nucleation and basal growth[16] or tip-led growth modes[17] for metal oxides at the synthesis temperatures. However, the metals under consideration here, such as tungsten, do not melt at the synthesis temperatures. So, the present case of chemical-vapor transport and deposition of metal oxide species for obtaining both metal and metal oxide nanowires falls into the category of CVD techniques with only gas–solid interactions and without the use of catalyst particles or templates. It is therefore important to understand the mechanisms responsible for 1D growth of both metal and metal oxide nanowires using only the vapor–solid schemes. We performed a systematic experimental study, followed by a thorough thermodynamic analysis, to clearly understand the nucleation and growth mechanisms involved in the nanowire formation. In addition, the above concept was investigated using nickel and tantalum filaments for synthesizing their respective oxide nanowires.

One of the primary uses for synthesized nanowire powders is with dispersions in several solvents; we therefore also studied the dispersion behavior of the as-synthesized nanowire powder using common solvents such as 1-methoxy 2-propanol and ethanol, and so on. A few studies have recently discussed the dispersion of nanowires in polar solvents.[18–19] Here, the agglomeration and stability behavior of tungsten oxide nanowires in different solvents was studied and compared to that of commercially obtained nanoparticles.

2. Results and Discussion

A set of experiments using the tungsten filament at a temperature of 1950 K and an oxygen partial pressure of 0.770 Torr resulted in the highest nucleation density (1.5×10^{10} cm^{-2}), leading to a vertical array of WO_3 nanowires on both quartz and fluorinated tin oxide (FTO) substrates. The substrate temperature under these conditions was measured to be between 775 and 823 K. The diameter of the nanowires obtained under these conditions ranged from 40 to 60 nm with lengths of a few micrometers (see Figure 1a and b for scanning electron microscopy (SEM) images of a vertical array of tungsten oxide nanowires on a quartz substrate). Under the same experimental conditions, nanowire arrays were synthesized on the FTO substrates and the as-synthesized nanowire arrays on the FTO substrates were tested for electrochromic devices; the results will be reported elsewhere.[20]

Another set of experiments performed at higher partial pressures of oxygen ($P = 10$ Torr), using the same substrate and filament temperatures, led to the formation of a high density of nanowires bundled in the form of ball-like structures. As shown in Figure 1c and d, the structures consisted of uniform-sized nanowires 20 nm in diameter and about 0.5 μm in length. A set of experiments performed by pulsing

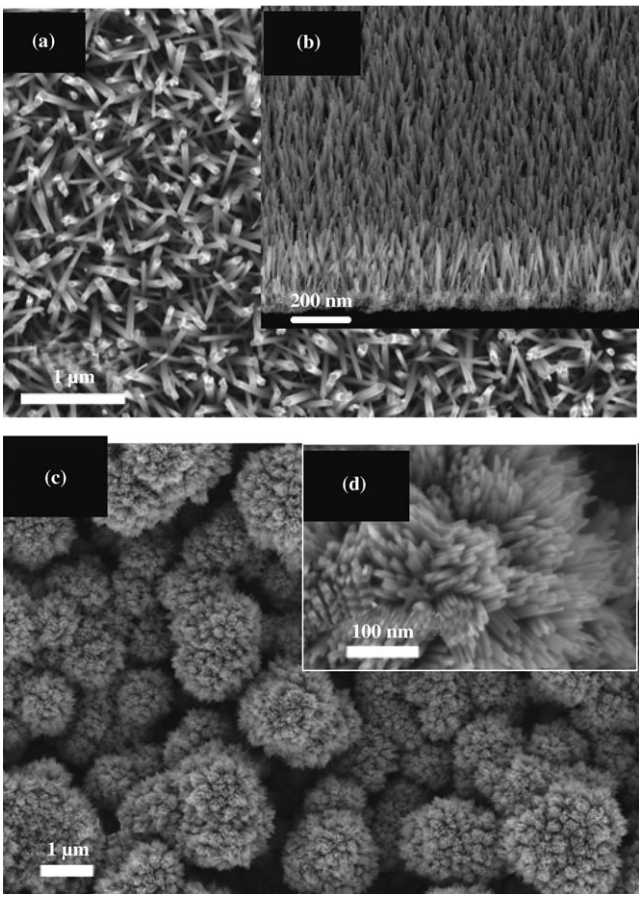

Figure 1. SEM images of as-synthesized, vertical arrays of tungsten oxide nanowires on the quartz substrate at a filament temperature of 1950 K. a) Low-magnification image showing individual nanowires with diameters in the range of 30 to 60 nm. b) Cross-sectional image of the as-synthesized, vertical arrays of nanowires on the FTO substrate. c) Low-magnification image showing the ball-like morphology of tungsten oxide nanowires obtained at high partial pressures of oxygen; the inset shows a higher-magnification image clearly indicating nanowires with uniform diameters of around 20 nm in each of the ball-like structures. d) High-magnification image clearly showing uniform-sized tungsten oxide nanowires in a single ball-like morphology of nanowires.

the oxygen flow rate of 8 to 0 sccm, with an off-time scale of a few minutes, repeated over three cycles resulted in 3D branched nanowires (see SEM images in Supporting Information). All other experimental parameters were kept constant: the filament temperature was 1950 K and the substrate temperature was around 775 to 823 K. The pulsing of oxygen flow allowed for secondary nucleation and resulted in the formation of branched nanowires.

The X-ray diffraction (XRD) spectrum (Figure 2a) indicated that the as-synthesized, bluish nanowire deposit was composed of an oxygen-deficient monoclinic $W_{18}O_{49}$ phase. Oxidation of the as-synthesized nanowires in an ambient atmosphere at a temperature of 773 K for about 30 min changed the color of the bluish nanowire deposit to yellow, and the corresponding XRD spectrum (Figure 2b) indicated that the phase of the nanowires changed from $W_{18}O_{49}$ to WO_3. At the same time, no structural damage or change

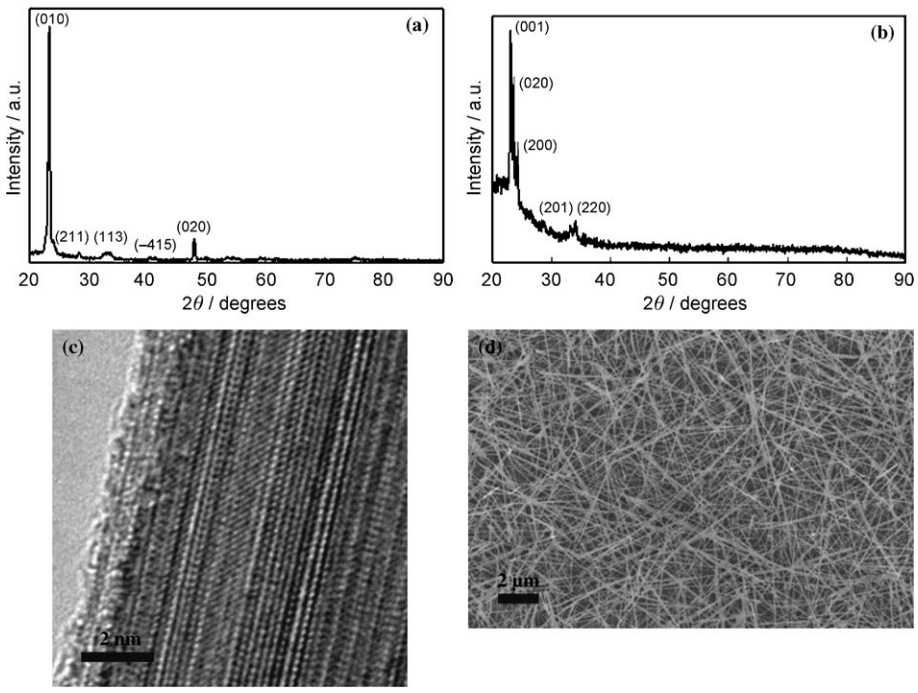

Figure 2. a) XRD spectra indicating that the as-synthesized tungsten oxide nanowires are made of the $W_{18}O_{49}$ phase. b) XRD spectra of the oxidized tungsten oxide nanowires indicating the WO_3 phase. c) HRTEM image showing the absence of an amorphous sheath on the surface of the nanowire. d) SEM image of blue deposit containing tungsten oxide nanowires with diameters around 40 nm and over 10 μm in length, obtained using partial pressure of oxygen of 0.4 Torr, a filament temperature of about 1950 K, and a substrate temperature of 800 °C.

was observed for nanowires after the oxidation. The Raman spectrum of tungsten oxide nanowires showed well-defined bands at 264, 322, 709, and 803 cm^{-1}. These bands correspond to the monoclinic tungsten oxide phase.[21] The Raman peaks at 264 and 322 cm^{-1} are assigned to the O–W–O bending modes, and the 709 and 803 cm^{-1} peaks are assigned to the stretching modes (see Supporting Information). As shown in Figure 2c, the high-resolution transmission electron microscopy (HRTEM) image of the nanowire shows no presence of amorphous sheath on the nanowire. The growth direction is determined to be [010], similar to the report in Reference [12].

Experiments were also conducted at a higher substrate temperature of 1073 K using the furnace around the quartz tube and an oxygen partial pressure of 0.4 Torr while maintaining the filaments at 1950 K. The as-synthesized blue deposition on the substrate showed a networked, nanowire thin film (or nanowire mat) containing 5-μm-long nanowires with diameters ranging from 20 to 70 nm. These nanowire mats consist of two phases: monoclinic $WO_{2.9}$ and tetragonal $WO_{2.8}$ (see Supporting Information). The experiments using the furnace around the quartz tube, a higher oxygen partial pressure of 4 Torr, and a substrate temperature of 1073 K resulted in a yellow–green deposit on the substrate that contained only nanoparticles and the corresponding WO_3 phase, as indicated by XRD measurements.

Experiments were performed to determine the effect of substrate temperature on the resulting nanowire density by varying the substrate temperature from 823 K to 1173 K, while keeping the filament temperature constant at 1950 K and using a constant partial pressure of oxygen ($P = 0.770$ Torr). As shown in Figure 3a, there is a decrease in the nanowire density with increasing substrate temperature. At higher substrate temperatures, lower supersaturation of gas-phase species results in nanowire mats. In all of the experiments performed, a uniform blue deposit was observed on both the FTO and the quartz substrates. Experiments were also performed at different partial pressures of oxygen, keeping the filament temperature ($T = 1950$ K) and the substrate temperature ($T = 823$ K) constant. As shown in Figure 3b, there is an increase in the nanowire density with increasing partial pressure of oxygen. In all experiments, a blue deposit gave an indication of nanowire formation and the yellowish green deposit gave an indication of nanoparticle formation.

The nucleation of tungsten oxide nanowires from the vapor phase could be understood further by considering the vapor-phase supersaturation. As shown in Figure 3c, the equilibrium conditions of the gas-phase species near the filament and the substrate were considered. The equilibrium calculations were performed using CHEMKIN 3.7.1 software (Reaction Design, Inc., CA) by considering various gas-phase species: O, O_2, WO, WO_2, W_3O_8, and WO_3, and solid-phase species: W, WO_2, $WO_{2.9}$, and WO_3. Thermodynamic data is not available for both solid- and gas-phase species of suboxides such as $W_{18}O_{48}$, $W_{18}O_{49}$, and so on. However, the W_3O_8 ($WO_{2.667}$) gas-phase species, similar to the experimentally observed $W_{18}O_{49}$ phase for nanowires, was included in the calculation. The equilibrium composition at the substrate is determined using the equilibrium composition from the filament as the initial composition. The gas-phase supersaturation is defined as the ratio of the partial pressure of a particular gas-phase species at the filament (P^*_f) to that at the substrate (P^*_S)as follows: supersaturation $= RT \ln (P^*_f/P^*_S)$.

At the experimental conditions ($T_f = 1950$ K), the absolute, equilibrium concentrations of both WO and W_3O_8 gas-phase species are found to be insignificant and need not be considered, and are about seven or more orders of magnitude less than that of the WO_2 gas-phase species. The supersaturations of WO_2 and WO_3 at various substrate temperatures are presented in Figure 4b. It can be easily observed that the supersaturation of WO_2 is much greater than that

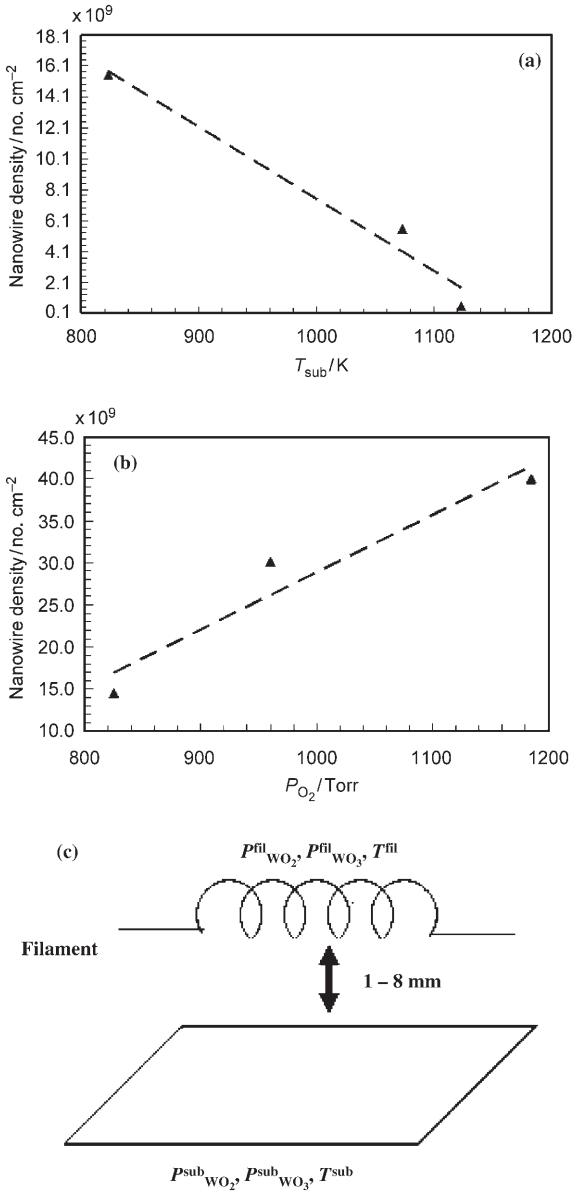

Figure 3. a) Experimental data showing the nanowire density obtained as a function of substrate temperature. b) Experimental data showing the effect of partial pressure of oxygen on the nanowire density at lower substrate temperature (823 K). c) Schematic image describing the equilibrium parameters at the filament and at the substrate used for estimating the imposed gas-phase supersaturation at the substrate.

of WO_3 under our experimental conditions; the WO_2 species are therefore expected to condense readily from the gas phase onto the substrate. Further, the condensation of WO_2 gas-phase species into solid WO_2 is thermodynamically favored. In the absence of knowledge of the reaction kinetics of oxygen decomposition at a tungsten filament, the amount of atomic oxygen is estimated to be negligible and we did not include any reactions involving atomic oxygen. The expected reactions involving WO_2 species are shown in Table 1 of the Supporting Information. The formation of gas-phase species of WO_2 is possible at the experimental conditions. Also, the condensation of WO_2 (gas, g) to WO_2 (solid, s), the desorption reaction and the oxidation reactions at the substrate are feasible (see Supporting Information).

Based on all of the possible reactions at the filament and the substrate, a nucleation and growth model, shown in Figure 4a, is proposed for the observed 1D growth of tungsten oxide nanowires: First, the high supersaturation of WO_2 (g) leads to condensation into WO_2 (s) clusters in a nucleation step. Secondly, further oxidation of WO_2 clusters could be favorable at the cluster–substrate interface, which leads to precipitation of WO_{3-x} crystals on the substrate with a tip whose dimensions are considerably less than the crystal. Finally, the enhanced adsorption of WO_2/WO_3 species on the tip relative to the bulk surface, followed by further oxidation at the cluster–crystal interface, leads to 1D growth of WO_{3-x} nanowires. The enhanced adsorption at the tip was also made possible by the competition between the net condensation reaction and the desorption/oxidation reactions on the WO_2 cluster in comparison to the WO_{3-x} nanowire, and determine the relative rates of axial versus radial growth. In essence, the nanowire nucleation could be through WO_2 cluster nucleation while 1D growth could be led by an amorphous WO_{2+y} cluster (with $2+y$ less than $3-x$) at the tip. The WO_{2+y} tip is not visible in any of the experimental results and it is presumed that the tip will also be oxidized during the experimental shutdown. Hence, there was no tip associated with tungsten oxide nanowires and the entire nanowire was composed of one phase, that is, the oxygen-deficient $W_{18}O_{49}$ phase.

If WO_2 species are responsible for nucleation, the nanowire density can be estimated as the following:

$$\text{Nanowire density} \propto RT\left[\ln\left(\frac{p_{WO_2,\text{filament}}}{p_{WO_2,\text{substrate}}}\right)\right]$$

As shown in Figure 3a, the nanowire density is inversely proportional to the substrate temperature, similar to the trend of WO_2 supersaturation as shown in Figure 4b. At higher substrate temperatures, the lower supersaturation of gas-phase species leads to the growth of low-density nanowires in the form of mats. At lower substrate temperatures, the higher supersaturation of gas-phase species leads to a high density of nucleation of nanowires that grew vertically in the form of arrays. At lower substrate temperatures, our thermodynamic computations predict that the equilibrium composition of WO_2 species in the gas phase becomes practically zero, which leads to extremely high supersaturation values. The experimentally calculated nanowire densities also correlate well with the estimated supersaturation trend at different partial pressures of oxygen (Figure 3b and Figure 4c). This explains the high nucleation densities observed at high partial pressures of oxygen.

Several synthesis experiments, in which the growth durations were varied from 10 to 60 min, were performed to determine the radial and axial growth rates of the nanowires. The results show that there was no increase in the density but an increase in both the diameter and length of the wires. A linear correlation was added and the intercept was

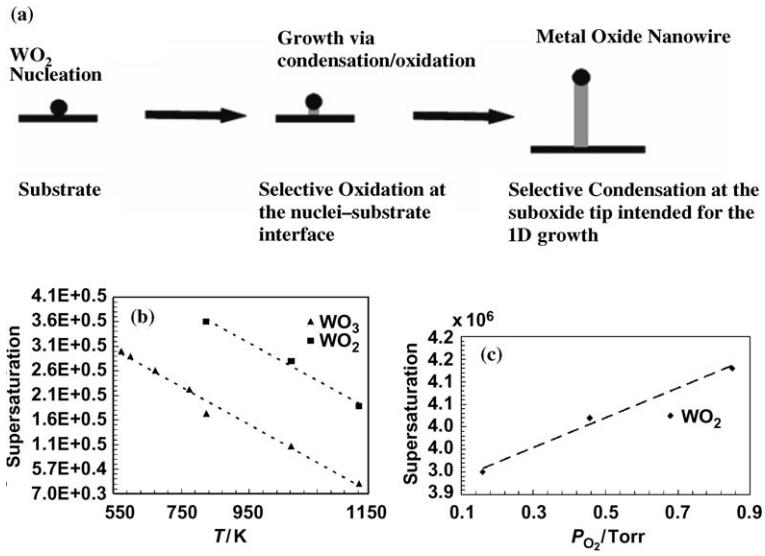

Figure 4. a) Schematic image illustrating the proposed mechanism for the formation of tungsten oxide nanowires through various solid–vapor interactions. b) Theoretically estimated supersaturation of tungsten oxide (WO_3 and WO_2) species as a function of substrate temperature. c) Theoretically estimated supersaturation of tungsten oxide (WO_2) species as a function of partial pressure of oxygen (at constant substrate temperature of 823 K and filament temperature of 1950 K).

made zero to approximate the growth rate (see Supporting Information). It was observed that the radial growth rate was 2.82 nm min^{-1} and the axial growth rate was 0.38 μm min^{-1}, which suggests an anisotropic growth-rate ratio of about 100. In some experiments, the aspect ratios of the resulting nanowires were as high as 1000. Such anisotropic growth in crystals could not be accounted for by the differences in growth rates expected in different crystallographic directions in a crystal. As proposed, a suboxide cluster at the tip promotes axial growth through enhanced adsorption of growth species. The proposal of oxide clusters for enabling 1D growth of nanowires is not completely new. It was first observed with silicon-nanowire growth in which suboxide silica (SiO_x) clusters at tips were hypothesized to be responsible for the observed 1D growth.[22] However, the SiO_x clusters at tips were not directly observed but a sheath of silica was observed around the crystalline silicon nanowires.[23] In a later study using direct oxidation of Si, it was also observed that silica nuclei aided in the 1D growth of amorphous silica nanowires.[24] Recently, we showed that the high density of nucleation and basal growth was found to be responsible for Nb_2O_5 nanowire growth under direct plasma oxidation of Nb foils in the absence of any foreign metal contamination.[25] In another study, a mixture of iron oxide and boron oxides promoted the growth of magnesium oxide nanowires, probably by providing the molten-phase clusters at the tip during synthesis.[26]

The experiments were also performed with the aim of demonstrating the concept for other metal oxide systems, using nickel and tantalum filaments. In both the cases, the respective metal oxide nanowires, that is, NiO and Ta_2O_5, were obtained. Representative SEM images and Raman spectra of the NiO and Ta_2O_5 nanowires are shown in Figure 5. The use of low amounts of oxygen in our synthesis conditions allowed for longer lifetimes of the filaments. In the case of tungsten filaments, the filaments typically lasted over several tens of experiments without causing any hot spots. The technique described here could easily be extended to several material systems beyond tungsten, nickel, and

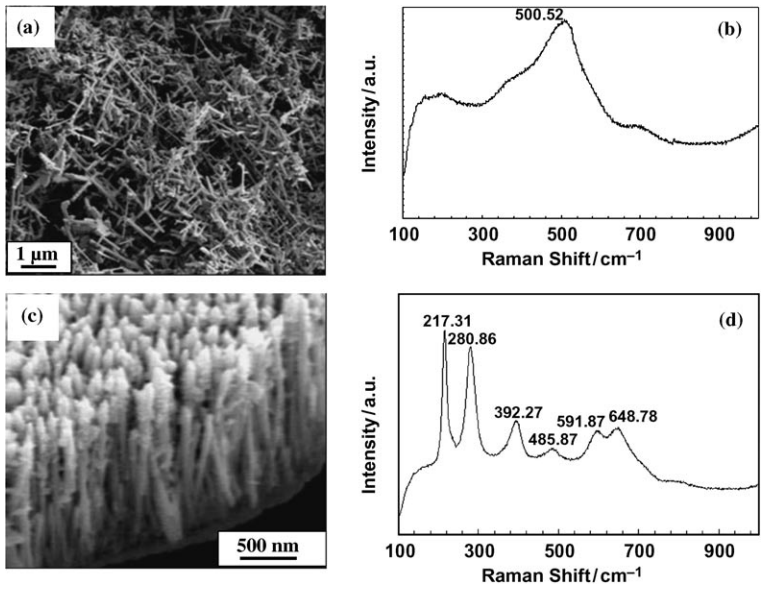

Figure 5. a) SEM image of NiO nanowires synthesized using the chemical-vapor transport concept with nickel as the hot filament (filament temperature = 1350 °C, 1 sccm O_2/100 sccm Ar). b) Raman spectrum of the as-synthesized nanowires showing a broad peak at 500.5 cm^{-1} that corresponds to the NiO phase. c) Ta_2O_5 nanowires synthesized using tantalum filaments (filament temperature = 2000 °C, 100 sccm Ar/0.4 sccm air), and d) Raman spectrum of the as-synthesized nanowire deposit showing primary modes corresponding to Ta_2O_5.

tantalum. Also, the technique could easily be scaled up by increasing the diameter of the quartz tube used. In the case of scale-up, the metal oxide nanowires could either be grown in the form of vertical arrays or could be scraped up easily for bulk quantities of nanowires. In either case, the resulting metal oxide nanowires do not contain any foreign metal contamination, allowing them to be used readily.

Interestingly, the as-synthesized nanowires exhibited stable dispersions in both organic and aqueous solvents such as dimethyl formamide (DMF) and water. The sedimentation studies of nanowire dispersions showed that the nanowires remain in the solution for longer periods of time and no sediment or any kind of agglomeration is noticed for long periods of time. Similar studies using commercially available, tungsten trioxide nanoparticles with a primary particle size of 30 nm showed that they form micrometer-sized spherical agglomerates that sediment out quickly. Typical SEM images (see Supporting Information) showed differences in the agglomeration patterns: In the case of nanowire dispersions, the sediment shows the randomly placed nanowires, indicating no agglomeration of nanowires in the solution; the nanoparticle dispersions show micrometer-scale, spherical aggregates containing the primary nanoparticles. The difference in their agglomeration behavior seems to be influenced mainly by their shape (high aspect ratio) as both as-synthesized nanowires and nanoparticles exhibit the same zeta-potential values.

3. Conclusions

In summary, we have presented a chemical-vapor transport method for the synthesis of large quantities of tungsten oxide nanowires with different morphologies (nanowire mats, nanowire arrays, branched structures, and ball-shaped morphologies containing nanowires) on various substrates. A thermodynamic model was proposed that suggests that the gas-phase supersaturation of WO_2 is responsible for the nucleation of WO_{3-x} nanowires and a WO_{2+y} ($2+y$ less than $3-x$) cluster at the tip is proposed to be responsible for nanowire growth. The proposed model predicted the large dependence of nanowire density on both the substrate temperature and partial pressures of oxygen, consistent with the experimental findings. In addition to tungsten oxide, this method is applicable in synthesizing nanowires of other transition metals, as demonstrated using nickel oxide and tantalum oxide as additional examples. Further, the scalability of the concept was also demonstrated and this concept could potentially be scaled-up further for inexpensively obtaining gram quantities of nanowires. The as-synthesized tungsten oxide nanowires formed stable dispersions in a variety of aqueous and organic solvents compared to nanoparticles.

4. Experimental Section

A hot-filament CVD reactor setup, equipped with the necessary metal-filament source, was employed for the synthesis of the metal oxide nanowires. The setup, shown in Figure 6a, consists of a 2-in.-diameter quartz tube housed in a tube furnace heater. For the synthesis of tungsten oxide nanowires, a 0.5-mm-diameter coiled tungsten filament was used as the source. The tungsten filament was heated to temperatures ranging from 1773–2273 K. The temperatures of both the filament and the substrate were monitored using a dual-wavelength pyrometer (Wilkinson, MA). Quartz boats were employed for collecting the deposition and preventing direct deposition onto the walls of the quartz tube. Typically, the substrates (quartz and FTO-coated quartz slides) were placed on the boat, as shown in the schematic. In the absence of the furnace, the radiation from the hot filaments directly heated the substrates to a maximum temperature of about 823 K. In some cases, furnace heating was employed to achieve higher substrate temperatures while maintaining the same filament temperature. The feed-gas composition was controlled using pure oxygen or argon/air mixtures for oxygen partial pressures ranging from 0.1 Torr to 10 Torr. The tungsten filament was always heated to a temperature of about 1950 K while maintaining the power (voltage and current used for heating the filament) constant in all of the experiments. The typical duration of each experiment was approximately 15 min. The optical photograph in Figure 6b shows quartz slides coated with tungsten oxide nanowire arrays uniformly over large areas.

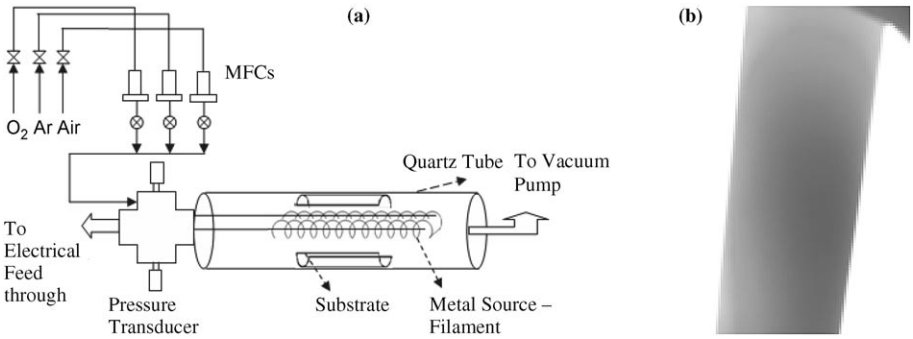

Figure 6. a) Schematic image of the hot-filament CVD reactor using tungsten filaments. MFC: mass-flow controller. b) Optical image showing the uniform coating of the tungsten oxide nanowire arrays on a quartz substrate.

The as-synthesized nanowires were collected in a dry powder form by scraping it from the quartz substrates. The as-obtained nanowire powder was dispersed into three different solvents: water, ethanol and 1-methoxy 2-propanol, and DMF using ultrasonication with a horn (UP200S Ultrasonic Processor) for two minutes, followed by sonication using an ultrasonication bath for

about 15 min. The dispersions were allowed to settle for a few minutes and the initial sediments were taken out and weighed. The intermittent sediments were examined using SEM to observe the agglomeration patterns.

Acknowledgements

The authors acknowledge the financial support of the Kentucky Science and Engineering Foundation (KSEF-148-502-04-86), Western KY Energy Consortium (MOU-OSP2005-026), the US Department of Energy for supporting the Institute for Advanced Materials (DE-FG02–05ER64071), Kentucky Renewable Energy Commission/US-DOE (DE-FG36–05G085013 A), and the University of Louisville for fellowship support to J. Thangala. Also acknowledged is Dr. Z. Chen at IAM-RE for help with HRTEM.

[1] C. C. Lia, F. R. Chen, J. J. Kai, *Sol. Energy Mater. Sol. Cells* **2006**, *90*, 1147 – 1155.
[2] C. J. Jin, T. Yamazaki, Y. Shirai, T. Yoshizawa, T. Kikuta, N. Nakatani, H. Takeda, *Thin Solid Films* **2005**, *474*, 255 – 260.
[3] E. L. Miller, B. Marsen, B. Cole, M. Lum, *Electrochem. Solid-State Lett.* **2006**, *9*, G248-G250.
[4] K. Liu, D. T. Foord, L. Scipioni, *Nanotechnology* **2005**, *16*, 10 – 14.
[5] H. Qi, C. Wang, J. Liu, *Adv. Mater.* **2003**, *15*, 411 – 414.
[6] Y. Jin, Y. Zhu, R. L. D. Whitby, N. Yao, R. Ma, P. C. P. Watts, H. W. Kroto, D. R. M. Walton, *J. Phys. Chem. A* **2004**, *108*, 15 572 – 15 577.
[7] S. J. Wang, C. H. Chen, R. M. Ko, Y. C. Kuo, C. H. Wong, C. H. Wu, K. M. Uang, T. M. Chen, B. W. Liou, *Appl. Phys. Lett.* **2005**, *86*, 263 103 – 263 106.
[8] K. Hong, W. Yiu, H. Wu, J. Gao, M. Xie, *Nanotechnology* **2005**, *16*, 1608 – 1611.
[9] Z. Liu, Y. Bando, C. Tang, *Chem. Phys. Lett.* **2003**, *372*, 179 – 182.
[10] Z. Xiao, L. Zhang, X. Tian, X. Fang, *Nanotechnology* **2005**, *16*, 2647 – 2650.
[11] J. Liu, Y. Zhao, Z. Zhang, *J. Phys. Condens. Matter* **2003**, *15*, L453 L461.
[12] G. Gu, B. Zheng, W. Q. Han, S. Roth, J. Liu, *Nano Lett.* **2002**, *2*, 849 – 851.
[13] Y. Q. Zhu, W. Hu, W. K. Hsu, M. Terrones, N. Grobert, J. P. Hare, H. W. Kroto, D. R. M. Walton, H. Terrones, *Chem. Phys. Lett.* **1999**, *309*, 327 – 334.
[14] Y. Li, Y. Bando, D. Golberg, *Adv. Mater.* **2003**, *15*, 1294 – 1296.
[15] S. Vaddiraju, H. Chandrasekaran, M. K. Sunkara, *J. Am. Chem. Soc.* **2003**, *125*, 10 792 – 10 793.
[16] S. Sharma, M. K. Sunkara, *J. Am. Chem. Soc.* **2002**, *124*, 12 288 – 12 293.
[17] S. Vaddiraju, A. Mohite, A. Chin, M. Meyyappan, G. Sumanasekera, B. W. Alphenaar, M. K. Sunkara, *Nano Lett.* **2005**, *5*, 1625 – 1631.
[18] V. Nicolosi, D. Vrbanic, A. Mrzel, J. McCauley, S. O'Flaherty, C. McGuinness, G. Compagnini, D. Mihailovic, J. W. Blau, N. J. Coleman, *J. Phys. Chem. A* **2005**, *109*, 7124 – 7133.
[19] F. L. Deepak, P. Saldanha, S. R. C. Vivekchand, A. Govindaraj, *Chem. Phys. Lett.* **2006**, *417*, 535 – 539.
[20] S. Gubbala, J. Thangala, M. K. Sunkara, *Sol. Energy Mater. Sol. Cells*, **2007**, DOI:10.1016/j.solmat.2007.01.016.
[21] C. Santato, M. Odziemkowski, M. Ulmann, J. Augustynski, *J. Am. Chem. Soc.* **2001**, *123*, 10 639 – 10 649.
[22] Y. F. Zhang, Y. H. Tang, H. Y. Peng, N. Wang, C. S. Lee, I. Bello, S. T. Lee, *Appl. Phys. Lett.* **1999**, *75*, 1842 – 1844.
[23] J. L. Gole, J. D. Stout, W. L. Rauch, Z. L. Wang, *Appl. Phys. Lett.* **2000**, *76*, 2346 – 2348.
[24] J. Q. Hu, Y. Jiang, X. M. Meng, C. S. Lee, S. T. Lee, *Chem. Phys. Lett.* **2003**, *367*, 339 – 343.
[25] M. Mozetic, U. Cvelbar, M. K. Sunkara, S. Vaddiraju, *Adv. Mater.* **2005**, *17*, 2138 – 2142.
[26] C. Tang, Y. Bando, T. Sato, *J. Phys. Chem. B* **2002**, *106*, 7449 – 7452.

Received: December 7, 2006
Revised: March 2, 2007
Published online on April 5, 2007